Report

Current Biology

A Cellular Insulator against CLE45 Peptide Signaling

Highlights

- OPS activity antagonizes CLE45 signaling in developing protophloem sieve elements
- Enhanced CLE45 signaling can be overcome by increased OPS dosage
- OPS dampens CLE45 sensing by direct interference with CLE45 signaling components
- OPS hyperactivity confers resistance to various root-active CLE peptides

Authors

Alice S. Breda, Ora Hazak, Patrick Schultz, Pauline Anne, Moritz Graeff, Rüdiger Simon, Christian S. Hardtke

Correspondence

christian.hardtke@unil.ch

In Brief

This study by Breda et al. reveals a novel mechanism in the quantitative modulation of CLE peptide signaling. The authors demonstrate that the *Arabidopsis* protein OPS promotes root protophloem differentiation by antagonizing autocrine CLE45 peptide signaling, through direct interference with the CLE45 signaling components BAM3 and CLV2|CRN.

Breda et al., 2019, Current Biology *29*, 2501–2508
August 5, 2019
https://doi.org/10.1016/j.cub.2019.06.037

CellPress

Current Biology
Report

A Cellular Insulator against CLE45 Peptide Signaling

Alice S. Breda,[1,3] Ora Hazak,[1,3] Patrick Schultz,[2,3] Pauline Anne,[1] Moritz Graeff,[1] Rüdiger Simon,[2] and Christian S. Hardtke[1,4,*]
[1]Department of Plant Molecular Biology, University of Lausanne, Biophore Building, 1015 Lausanne, Switzerland
[2]Institute for Developmental Genetics and Cluster of Excellence on Plant Sciences, Heinrich Heine University, 40225 Düsseldorf, Germany
[3]These authors contributed equally
[4]Lead Contact
*Correspondence: christian.hardtke@unil.ch
https://doi.org/10.1016/j.cub.2019.06.037

SUMMARY

Plants continuously elaborate their bodies through post-embryonic, reiterative organ formation by apical meristems [1]. Meristems harbor stem cells, which produce daughter cells that divide repeatedly before they differentiate. How transitions between stemness, proliferation, and differentiation are precisely coordinated is not well understood, but it is known that phytohormones as well as peptide signals play important roles [2–7]. For example, in *Arabidopsis thaliana* root meristems, developing protophloem sieve elements (PPSEs) express the secreted CLAVATA3/EMBRYO SURROUNDING REGION-RELATED 45 (CLE45) peptide and its cognate receptor, the leucine-rich repeat receptor kinase (LRR-RK) BARELY ANY MERISTEM 3 (BAM3). Exogenous CLE45 application or transgenically increased CLE45 dosage impairs protophloem formation, suggesting autocrine inhibition of PPSE differentiation by CLE45 signaling. Since CLE45 and BAM3 are expressed throughout PPSE development, it remains unclear how this inhibition is eventually overcome. The *OCTOPUS* (*OPS*) gene is required for proper PPSE differentiation and therefore the formation of continuous protophloem strands. OPS dosage increase can mend the phenotype of other mutants that display protophloem development defects in association with CLE45-BAM3 hyperactivity [8, 9]. Here, we provide evidence that OPS protein promotes differentiation of developing PPSEs by dampening CLE45 perception. This markedly quantitative antagonism is likely mediated through direct physical interference of OPS with CLE45 signaling component interactions. Moreover, hyperactive OPS confers resistance to other CLE peptides, and ectopic OPS overexpression triggers premature differentiation throughout the root. Our results thus reveal a novel mechanism in PPSE transition toward differentiation, wherein OPS acts as an ''insulator'' to antagonize CLE45 signaling.

RESULTS AND DISCUSSION

A. thaliana root meristems display a stereotypical morphology [10, 11]. Stem cells at the root tip produce daughter cells that divide repeatedly to generate cell files, which acquire distinct tissue identities depending on their position. The balance between cell production and timing of differentiation determines root meristem size and growth rate and is coordinated by intersecting hormone and peptide signals [3, 6, 12–17]. Exogenous application of many CLE peptides suppresses root growth [13, 18–20]. Sensing of these so-called root-active CLE peptides requires the receptor-like protein CLAVATA2 (CLV2) and the CORYNE (CRN) pseudokinase in the protophloem [21]. CLV2 and CRN function as a heteromer (CLV2|CRN) and are interdependent for their efficient plasma membrane recruitment [22, 23].

Protophloem is critical for meristem maintenance [8, 24, 25]. Differentiating protophloem sieve elements (PPSEs) undergo major cellular rearrangements, such as cell-wall buildup and nucleus degradation [8, 26]. In *brevis radix* (*brx*) and *ops* mutants, PPSEs frequently fail to differentiate. Such cells appear as ''gaps'' that interrupt protophloem strand continuity and thereby obstruct efficient phloem sap delivery to the meristem [8, 9]. *brx* or *ops* defects can be rescued by *bam3* second site mutations [8, 18, 21]. Conversely, CLE45 peptide application or dosage increase suppresses PPSE differentiation, suggesting a role for autocrine peptide signaling in protophloem formation [8, 18, 27, 28]. Moreover, CLE45 signaling through BAM3 is quantitatively limited by the CLV2|CRN heteromer [21], which is why *crn* mutants are resistant to CLE45.

BRX and OPS are plant-specific plasma membrane-associated, polar proteins [8, 9]. BRX localizes rootward, where it modulates auxin flux [29], whereas OPS localizes shootward. The molecular mode of OPS action remains largely obscure. Ectopic overexpression of OPS triggers severe developmental phenotypes [30, 31], which could be explained by OPS interference with brassinosteroid signaling in the case of hypocotyl elongation [30]. However, a pertinent OPS deletion variant can still complement the *ops* root protophloem phenotype [31, 32]. The most remarkable feature of OPS is its strongly quantitative action [31]. For example, OPS gain-of-function mutations as well as increased OPS dosage can rescue *brx* protophloem (and thus root growth) defects [8, 28, 31].

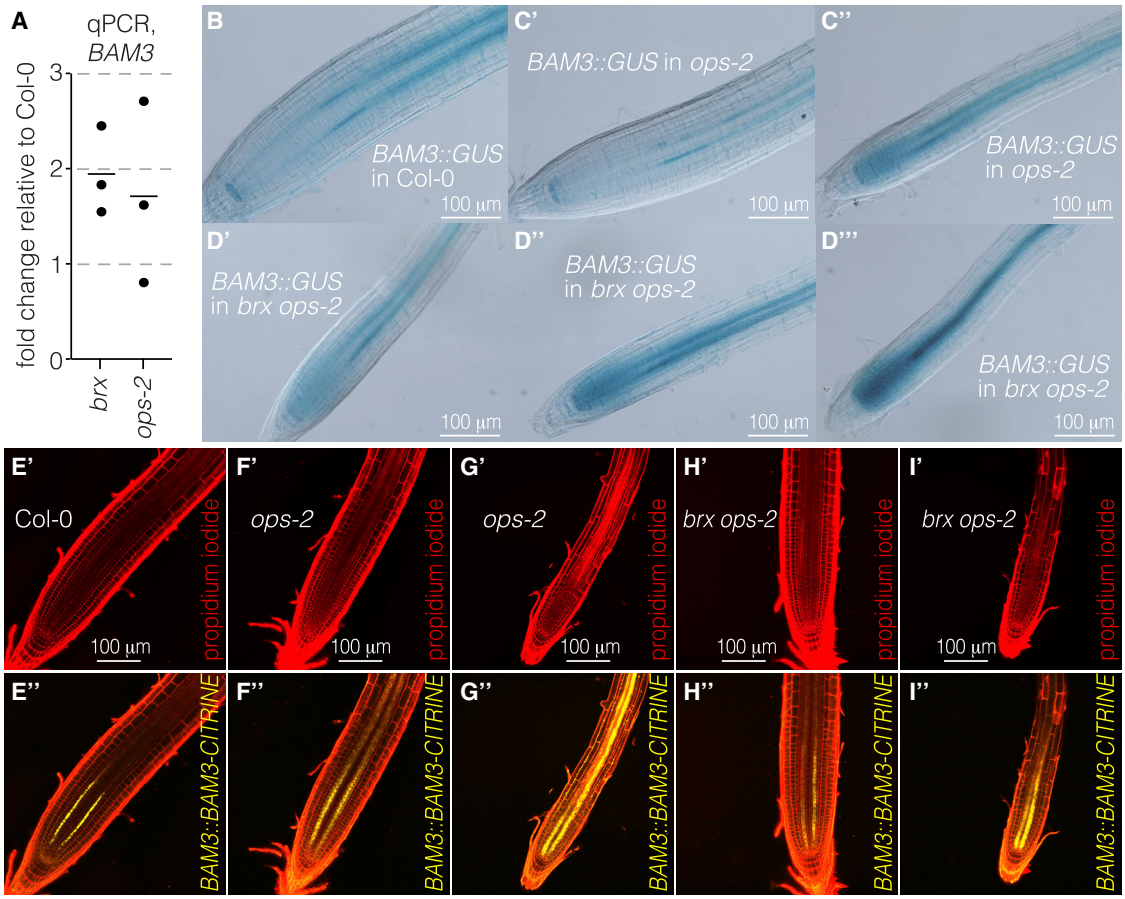

Figure 1. *BAM3* Expression in *ops* Loss-of-Function Mutants

(A) Expression level of *BAM3* mRNA in primary root tips of *Arabidopsis brx* or *ops* loss-of-function mutants, determined by quantitative real-time PCR as compared to Col-0 wild type (3 technical replicates each for 3 biological replicates; bar, mean).

(B–D) Detection of beta-glucuronidase (GUS) reporter activity expressed under control of *BAM3* promoter in root tips of indicated genotypes. Representative roots for Col-0 (B) and mutant individuals of different phenotypic severity (C and D) are shown.

(E–I) Detection of BAM3-CITRINE fusion protein expressed under control of *BAM3* promoter in root tips of indicated genotypes. Representative roots for Col-0 (E) and mutant individuals of different phenotypic severity (F–I) are shown. Top panels: cell outlines revealed by propidium iodide (PI) cell-wall staining, red fluorescence. Bottom panels: the BAM3-CITRINE fluorescence signal (yellow) merged with the PI signal in 7-day-old seedlings.

Quantitative Antagonism between CLE45 Signaling and OPS Determines Protophloem Differentiation

BAM3 transcription is elevated in *brx* root tips [18], which we confirmed by qPCR and also observed in *ops* loss-of-function mutants (Figure 1A). Interestingly, however, GUS reporter expression under control of the *BAM3* promoter (*BAM3::GUS*) varied in *ops* mutants and correlated with the stochastic range of phenotypic severity (Figures 1B and 1C). Similar variation was observed in *brx ops* double mutants, although they generally expressed *BAM3::GUS* at higher level (Figure 1D). These observations were confirmed with BAM3-CITRINE fusion protein (*BAM3::BAM3-CITRINE*) (Figures 1E–1I). Thus, *BAM3* expression varied across mutant individuals and higher levels correlated with a stronger phenotype. Moreover, expression was overall higher in *brx ops* double mutants, consistent with reported additive effects of *brx* and *ops* loss of function [31].

A semi-dominant *ops* second site mutation, ops^{E319K}, renders OPS hyperactive and can partially rescue *brx* mutants [8, 31]. Even more intriguing, *brx* mutants are frequently fully rescued by introduction of an *OPS::OPS-GFP* transgene ($brx^{OPS::OPS\text{-}GFP}$) [8]. Since ops^{E319K} roots also display resistance to CLE45 application [8], we explored whether *brx* rescue by *OPS* gain of function or dosage increase could reflect a role of *OPS* in antagonizing CLE45 perception. Indeed, *brx* ops^{E319K} double mutants were slightly CLE45-resistant, although less so than ops^{E319K} single mutants (Figure 2A), with the caveat that these genotypes are difficult to compare because protophloem defects are only partially restored in *brx* ops^{E319K} double mutants. In contrast, both protophloem development and root growth were normal in most $brx^{OPS::OPS\text{-}GFP}$ seedlings. Yet while roots of the transgenic Col-$0^{OPS::OPS\text{-}GFP}$ wild type were strongly CLE45-resistant, this was barely the case for $brx^{OPS::OPS\text{-}GFP}$ seedlings (Figure 2B). Moreover, CITRINE fusions of differentially active OPS variants [31] conferred varying degrees of CLE45 resistance in Col-0 as well as *ops* backgrounds, but less so, if at all, in *brx ops* double mutants (Figure 2C). Thus, overall the extent of CLE45 resistance was a function of the overlay between *OPS* gene dosage and/or protein activity and the

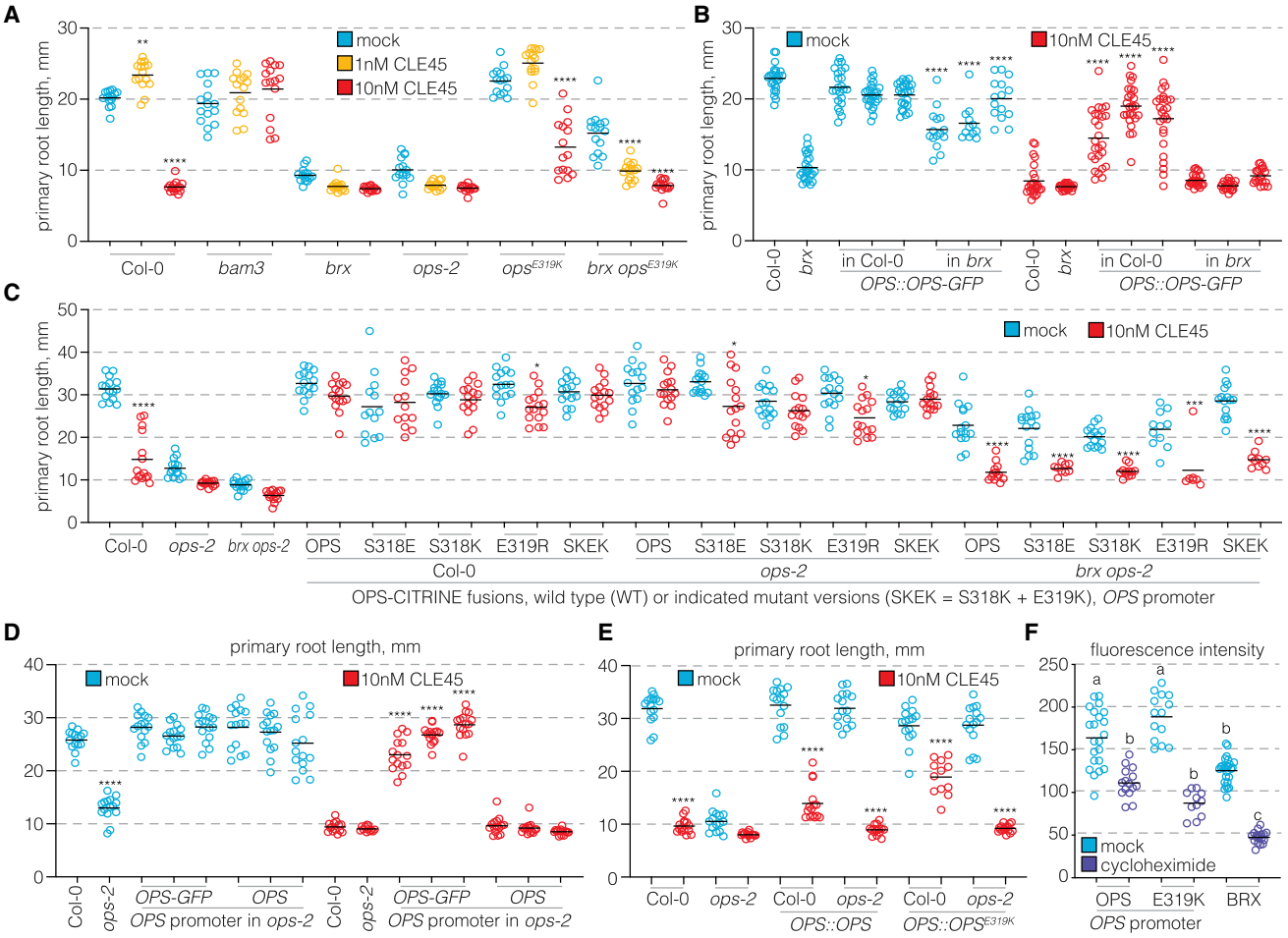

Figure 2. Quantitative, Background-Dependent CLE45 Resistance Conferred by OPS Gain of Function

(A) Root length of indicated genotypes on media supplemented with CLE45 peptide. Note that *ops-2* is a loss-of-function allele, while *ops*^{E319K} is a gain-of-function allele. The statistically significant difference compared to mock is indicated.

(B) CLE45 response of seedlings that carry an *OPS::OPS-GFP* transgene in Col-0 or *brx* background (three independent lines per transgene, comparable expression levels). The statistically significant difference compared to background is indicated.

(C) CLE45 response of transgenic seedlings that express indicated OPS variants in different backgrounds (representative lines). The statistically significant difference compared to mock is indicated.

(D) CLE45 response of transgenic seedlings that express indicated transgenes in *ops* background (three independent lines per transgene). The statistically significant difference compared to Col-0 is indicated.

(E) CLE45 response of seedlings that carry indicated transgenes in Col-0 or *ops* loss-of-function background (representative lines). The statistically significant difference compared to mock is indicated.

(F) Quantification of fluorescence in roots upon 1 h mock or 50 μM cycloheximide treatment, for OPS-GFP fusion proteins and BRX-CITRINE fusion protein (averages of 11–22 roots, 10–20 cells per root).

Seven-day-old seedlings. Plots display individual values (dots) and the mean (bar). *p < 0.05; ***p < 0.001; ****p < 0.0001; see also Figures S1 and S2 and Data S1 for statistical test details.

presence or absence of *BRX*. Our observations therefore suggest that antagonism between CLE45 signaling and OPS action is sensitive to quantitative variation and plays an important role in PPSE differentiation.

C-Terminal Fusions Impact OPS Activity

We previously observed that fluorescent tags impact OPS activity [31]. To determine whether tags also affect the ability of *OPS* to antagonize CLE45 signaling, we tested Col-0$^{OPS::OPS}$ and Col-0$^{OPS::OPS\text{-}GFP}$ lines. Indeed, compared to the GFP-tagged version, untagged OPS conferred less CLE45 resistance (Figure 2D). Yet again, untagged OPS^{E319K} conferred stronger resistance than untagged OPS (Figure 2E). Moreover, although both untagged transgenes complemented *ops* mutants, they conferred hardly any resistance in this background (Figures 2D and 2E), reiterating the importance of total OPS dosage in antagonizing CLE45 signaling. Interestingly, the impact of the fluorescent tags was not related to their size, since HA- or FLAG-epitope-tagged OPS versions were also relatively stronger agents than untagged OPS (Figure S1B). Thus, in general, C-terminal extensions amplified OPS activity. In summary, we can conclude that a combination of expression

level and protein activity determines overall OPS capacity to antagonize CLE45 signaling, reiterating the highly quantitative action of OPS [31].

Previous analyses suggested that OPS protein is turned over rapidly [31]. In cycloheximide-treated *OPS::OPS-GFP* seedlings, the OPS-GFP signal disappeared indeed swiftly (Figure 2F). This could neither be counteracted by protease inhibitor nor by proteasome inhibitor treatment (Figure S1C). Although it remains unclear whether our assays reflect realistic turnover because of the influence of the GFP tag, we could confirm the notion that OPS is rather unstable [31]. The mutated site in OPS^{E319K} apparently influences the phosphorylation state of a neighboring phosphoserine (S318) [31]. S318 seems to play a role in OPS turnover, because an OPS^{S318A} variant is much less abundant than wild-type OPS [31]. However, corroborating that gain-of-function alleles in this phosphosite do not notably affect OPS protein levels [31], no significant difference in relative turnover was observed for OPS^{E319K} (Figure 2F). Thus, OPS^{E319K} is apparently not hyperactive because of increased protein stability.

Alleviation of CLE45 Signaling Partially Rescues *ops* Phenotypes

Consistent with the observed antagonism between OPS and CLE45-BAM3, the *ops* phenotype can be fully rescued by *bam3* second site mutation [8, 18]. However, *BAM3::NLS-3XVENUS* transgene expression was not altered in ops^{E319K} roots (Figure S2A), suggesting that ops^{E319K} mutants are not CLE45-resistant due to reduced *BAM3* levels. Therefore, increased OPS activity might confer CLE45 resistance through post-transcriptional mechanisms. Because the CLV2|CRN heteromer is necessary for full CLE45 sensing in the protophloem [21], second-site *crn* mutation partially rescues *brx* root meristem size and growth [21]. We observed the same for *crn ops* double mutants (Figures S2B and S2C). However, although *brx crn* and *crn ops* phenotypes were on average less severe and meristems without defects in tendency more frequent, in aggregate protophloem gap frequencies were not significantly reduced (Figures S2D and S2E). In part, this could be explained by the larger meristems of the double mutants, which renders gaps more easily recognizable. Yet in summary, reduction of CLE45 signaling through *CRN* knockout could not compensate for reduced *OPS* activity to the same extent as *BAM3* mutation, suggesting quantitatively different roles of CRN and BAM3 in CLE45 response.

OPS Can Interact with CLE45 Signaling Components

To explore whether OPS might directly interfere with CLE45 perception, we sought to determine whether OPS can interact with CLE45 signaling components. Because our proteins of interest are either mainly plasma membrane-integral or -associated, we chose *in vivo* FRET-FLIM to investigate this question. Efficient CRN plasma membrane localization requires its heteromerization with CLV2 [22, 23]; thus, we first tested whether the presence of OPS changes the interaction dynamics between CRN and CLV2. To this end, *Nicotiana benthamiana* leaves were transiently transformed with fluorescent fusion proteins expressed under a constitutive promoter. In these assays, CRN-CFP fluorescence lifetime in presence of CLV2-CITRINE was further reduced by OPS-CITRINE co-expression (Figure S3A), indicating that OPS could interact with the CLV2|CRN complex. To confirm this notion, we switched to an inducible system that permits controlled expression timing and levels. In presence of untagged CLV2, we observed reduced fluorescence lifetime of CRN-GFP upon OPS-mCHERRY co-expression (Figure 3A), again indicative of interaction. Moreover, CRN-GFP fluorescence lifetime was significantly reduced upon BAM3-mCHERRY co-expression, but not upon co-expression of another plasma membrane-integral LRR-RK fusion, FLAGELLIN-SENSITIVE 2 (FLS2)-mCHERRY (Figure 3A). These results were confirmed in a reverse setup that monitored BAM3-GFP fluorescence lifetime (Figure S3B). Further, interaction of CRN with BAM3 and OPS was also observed in yeast split ubiquitin assays (Figure S3C). In summary, our results suggest that known CLE45 signaling components can interact with each other as well as with OPS *in vivo*.

OPS Can Interfere with CLE45 Signaling Component Interactions

Engineering increasingly positive charge into the OPS phosphosite creates progressively more active OPS variants [31], as exemplified by ops^{E319K}. To check whether this could alter interaction strength with CLV2|CRN, we included the strongest OPS variant, S318K E319K (OPS^{SKEK}), in our *N. benthamiana* FRET-FLIM assays. Compared to wild-type OPS, interaction between CRN and OPS^{SKEK} appeared to be more robust and somewhat stronger, but not in all replicate experiments, and not at statistically significant levels (Figure 3A). Thus, OPS^{SKEK} hyperactivity can likely not be explained by an increased propensity to interact with CLV2|CRN. We also determined whether the presence of CLE45 changes the quality or strength of any of the observed interactions, which was, however, not the case (Figure 3B).

Finally, we sought to monitor the dynamics of all four proteins upon simultaneous expression. Fluorescence lifetime reduction of constitutively expressed CRN-GFP in presence of untagged CLV2 and constitutively expressed BAM3-mCHERRY confirmed the proposed interaction between CRN and BAM3 (Figure 3C). However, this reduction was prevented by simultaneously induced co-expression of an OPS-CERULEAN fusion protein. These observations were confirmed in an alternative setup, where fluorescence lifetime of constitutively expressed CRN-GFP (in presence of untagged CLV2) could be reduced by induced BAM3-mCHERRY co-expression, but the effect could be reversed by simultaneous OPS-CERULEAN induction (Figures 3C and S3D). In summary, these results suggest that OPS can interfere with interactions between CLE45 signaling components. Because of the comparable abundance of the different proteins in the protophloem (Figures S3E–S3H), such interference likely affects CLE45 perception. To further characterize the interference, we conducted additional assays with a BAM3 deletion variant that lacked the intracellular kinase domain (but not the entire intracellular domain). This $BAM3^{\Delta KD}$-mCHERRY fusion protein still interacted with CRN-GFP, as well as with a CRN deletion variant that lacked the intracellular pseudokinase domain ($CRN^{\Delta PKD}$-GFP) (Figure 3D). Therefore, interaction between BAM3 and CLV2|CRN appears to be mediated by the extracellular and/or transmembrane domains. The $BAM3^{\Delta KD}$-mCHERRY interaction with CRN-GFP could still be disturbed by simultaneous OPS-CERULEAN expression. However, this

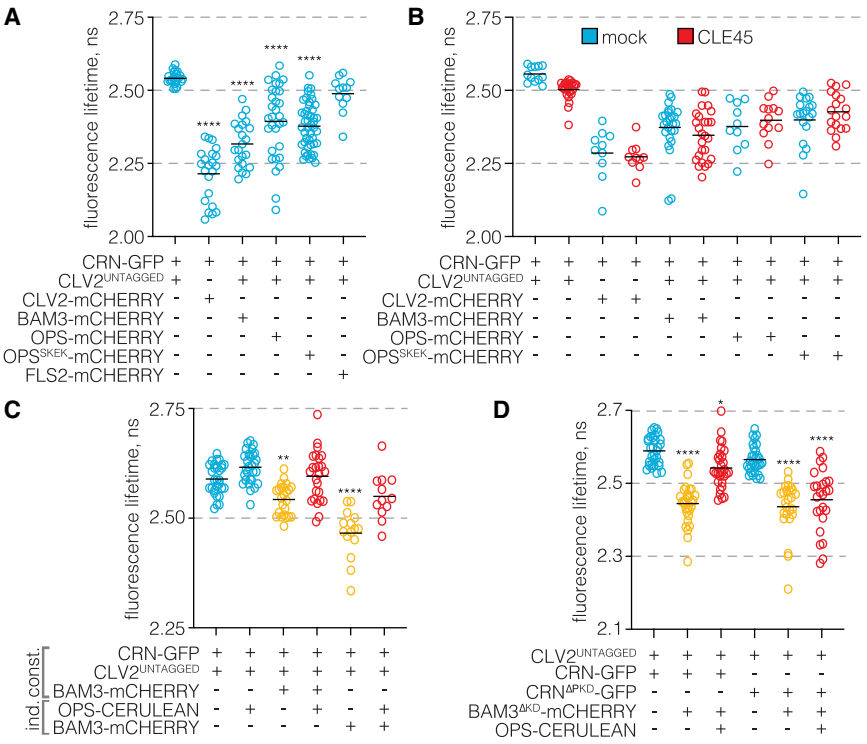

Figure 3. Protein-Protein Interactions between CLE45 Signaling Components and OPS

(A) FRET-FLIM measurements of CRN-GFP in combination with indicated fusion proteins expressed in transiently transformed *N. benthamiana* cells, under inducible promoter. The statistically significant difference compared to CRN-GFP + untagged CLV2 control is indicated.

(B) *N. benthamiana* FRET-FLIM measurements as in (A) after mock or CLE45 infiltration (no significant differences between treatments).

(C) *N. benthamiana* FRET-FLIM measurements of constitutively expressed CRN-GFP in presence of untagged CLV2, in combination with constitutive or induced BAM3-mCHERRY, and induced OPS-CERULEAN expression. The statistically significant difference compared to CRN-GFP + untagged CLV2 control is indicated.

(D) *N. benthamiana* FRET-FLIM measurements of induced CRN-GFP or a deletion variant that lacks the intracellular pseudokinase domain ($CRN^{\Delta PKD}$-GFP) in presence of untagged CLV2, in combination with induced BAM3-mCHERRY in presence or absence of induced OPS-CERULEAN expression. The statistically significant difference compared to CRN-GFP or $CRN^{\Delta PKD}$-GFP + untagged CLV2 controls is indicated.

Plots display individual values (dots) and the mean (bar). $^{**}p < 0.01$; $^{****}p < 0.0001$; see also Figure S3 and Data S1 for statistical test details.

was no longer the case when CRN-GFP was replaced by $CRN^{\Delta PKD}$-GFP (Figure 3D). These results suggest that OPS interferes with the interaction between BAM3 and CRN through binding to their intracellular domains, thereby quantitatively dampening CLE45 perception in a likely non-linear manner.

OPS Gain of Function Confers Resistance to Various Root-Active CLE Peptides

The results from the interaction assays were in line with the genetic hierarchy and suggest that OPS limits CLV2|CRN activity, which in turn quantitatively promotes BAM3 activity. Moreover, while BAM3 is specific for CLE45 in the root [18, 33], CLV2|CRN is required to sense various root-active CLE peptides [14, 21, 34, 35]. Therefore, if OPS can interfere with receptor interactions of CLV2|CRN, our results predicted that OPS gain of function might to some degree also interfere with sensing of other root-active CLE peptides. Indeed, ops^{E319K} mutants exhibited some resistance to application of a range of CLE peptides (Figures 4A and 4B). The extent of resistance was, however, variable and, unlike resistance of *crn* mutants monitored in parallel, not observed for all CLE peptides tested (8 out of 13). Moreover, CLE resistance of ops^{E319K} mutants was always weaker than CLE resistance of *crn* mutants (Figures 4A and 4B). These data are consistent with the idea that OPS can quantitatively interfere with CLV2|CRN activity and thereby modulate signaling strength of various CLE pathways.

Ectopic OPS Overexpression Promotes Early Differentiation

OPS is specifically expressed in the root protophloem [8, 9]. However, redundant, conserved OPS homologs exist [9, 31, 36], and in pertinent loss-of-function double mutants the *ops* phenotype is aggravated [36]. Consistent with suppression of protophloem differentiation by CLE peptides [21, 27, 28] and a role for OPS in antagonizing CLE signaling, these double mutants display substantial delays and frequent failures in protophloem differentiation [36]. Although the strong systemic impact of discontinuous protophloem strands on overall root meristem activity [24, 28] renders interpretation of these phenotypes difficult, the observed differentiation delays could be viewed as reduced capacity of developing PPSEs to escape the meristematic stage.

Whether conversely a strong increase in OPS activity can render plants even more resistant to CLE peptides remains unclear, because ectopic overexpression of OPS has severe consequences on root as well as shoot development [30, 31]. For instance, plants that express OPS-CITRINE fusions proteins under control of *UBIQUITIN 10* (*UBQ10*) promoter exhibit a variable growth phenotype, *in extremis* resulting in severely dwarfed plants that cannot complete their life cycle. Reemphasizing the highly quantitative nature of OPS action, phenotypic severity is also a function of transgene overexpression level [31]. This could be observed in the progeny of hemizygous *UBQ10::OPS-CITRINE* plants with moderate expression level, which segregated various root meristem phenotypes, ranging from nearly wild type to severely impaired growth (Figures 4C–4F), whereby phenotypic severity correlated with increased OPS-CITRINE level (Figures S4A and S4B). Yet, phenotypic severity was *a priori* not associated with apparent patterning defects. Rather, increased OPS-CITRINE correlated with earlier, sometimes nearly immediate PPSE elongation and differentiation (Figure 4G). Moreover, reduction of the meristematic state was essentially observed across all cell layers. For instance, cortex

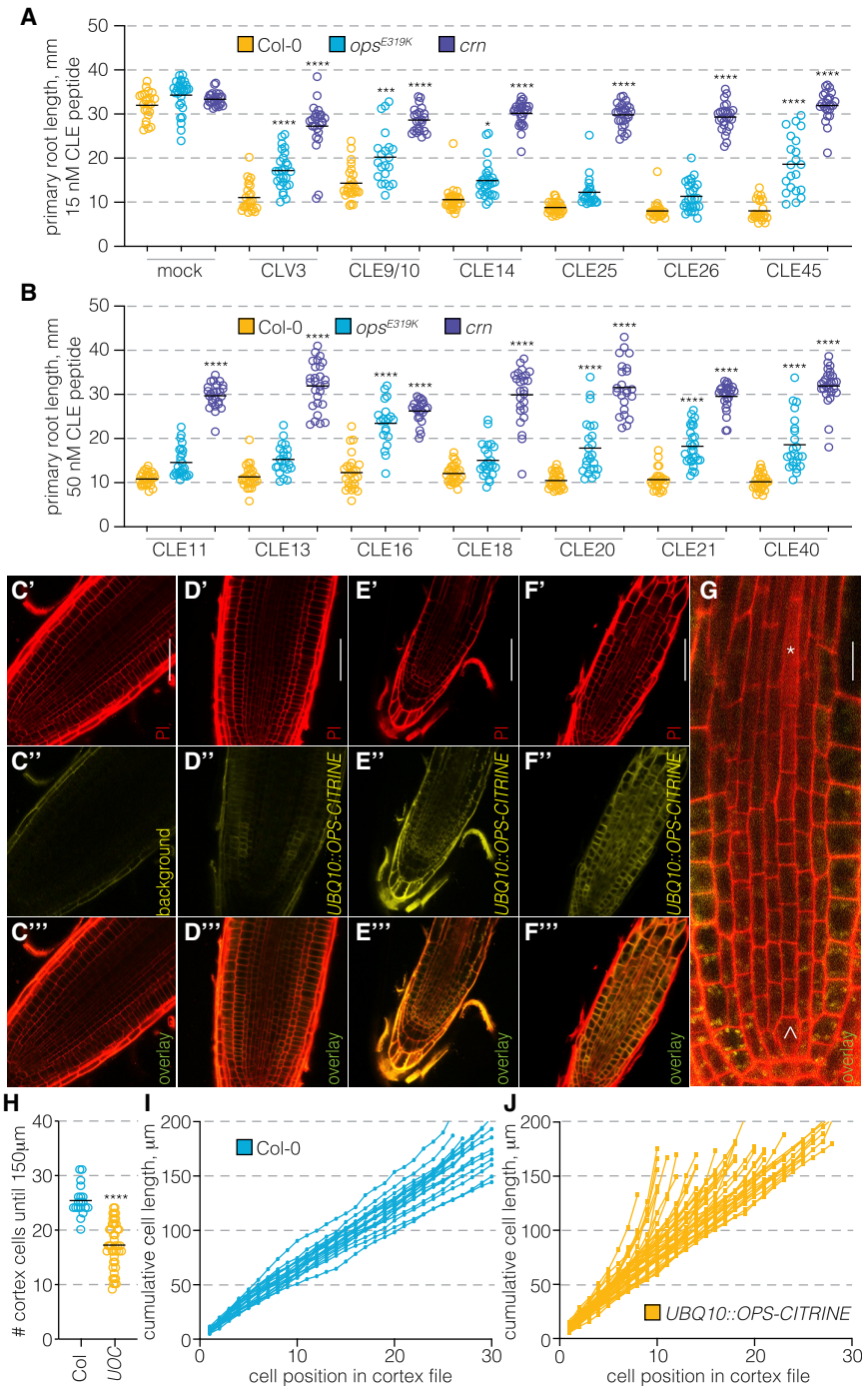

Figure 4. Developmental Consequences of OPS Hyperactivity

(A and B) Response of Col-0, *ops*^{E319K} and *crn* seedlings to efficient concentrations (15 nM in A; 50 nM in B) of various root active CLE peptides. The statistically significant difference compared to Col-0 is indicated.

(C–F) Phenotypic variation in the progeny of a hemizygous transgenic line as a function of the constitutive expression level of OPS-CITRINE fusion protein. Col-0 wild type is shown in (C). (D), (E) and (F) show different seedlings segregating from a hemizygous *UBQ10::OPS-CITRINE* mother plant. Note that confocal settings in (C′′)–(F′′) were not the same, due to the very strong CITRINE signals in (E′′) and (F′′).

(G) Accelerated protophloem differentiation from stem cell (arrowhead) to mature PPSE (asterisk) upon OPS-CITRINE overexpression.

(H) Number of cells in the first 150 µm of cortex cell files, starting from the stem cell daughter. UOC, *UBQ10::OPS-CITRINE* transgenic plants.

(I and J) Cumulative cell length in individual cortex cell files of Col-0 (I) or *UBQ10::OPS-CITRINE* (J) plants. Note frequently early cell elongation in *UBQ10::OPS-CITRINE* transgenic plants.

Seven-day-old seedlings. Plots display individual values (dots) and the mean (bar). ***p < 0.001; ****p < 0.0001; see also Figure S4 and Data S1 for statistical test details.

cells entered differentiation-elongation markedly earlier than in wild type (Figures 4H–4J), in extreme cases as early as one or two divisions after the initial stem cell division. One tangible interpretation of our results is that OPS ectopic overexpression accelerates the transition from proliferation to differentiation in protophloem as well as other root tissues.

Conclusion

Collectively, our findings support a scenario where OPS antagonizes CLE45 perception by direct interference with CLE45 signaling. This process is highly sensitive to quantitative perturbations on both sides. How this antagonism plays out along the protophloem to guide developing PPSEs from proliferation to differentiation remains unclear at this point. All the components identified in this network so far are expressed from the beginning to the end of PPSE development; thus, post-translational modifications might play an important role. For instance, OPS activity could be modulated by differential phosphorylation during PPSE ontogeny. Novel biochemical and cell biological tools will be necessary to comprehensively address this question in future studies. Yet from the genetic and cell biological data at hand, we can conclude that OPS is a key antagonist of BAM3 and CLV2|CRN, thereby acting as a "cellular insulator" against CLE45 signaling.

STAR★METHODS

Detailed methods are provided in the online version of this paper and include the following:

- KEY RESOURCES TABLE
- LEAD CONTACT AND MATERIALS AVAILABILITY

SUPPLEMENTAL INFORMATION

Supplemental Information can be found online at https://doi.org/10.1016/j.cub.2019.06.037.

ACKNOWLEDGMENTS

This work was supported by SNSF grant 31003A_166394 (awarded to C.S.H.), a DFG post-doctoral fellowship (awarded to M.G.), EMBO long-term post-doctoral fellowship ALTF 480-2016 (awarded to P.A.), and by the DFG through SFB1208 (awarded to R.S.). We would like to thank Dr. P. Cattaneo for the *BAM3::NLS-3XVENUS* construct, as well as Dr. J.-C. Palauqui and Prof. E. Farmer for sharing materials to perform yeast split ubiquitin assays.

AUTHOR CONTRIBUTIONS

A.S.B., P.A., and C.S.H. conceived and designed this project. A.S.B., O.H., P.S., P.A., and M.G. designed and performed the experiments. O.H. and C.S.H. drafted the manuscript. All authors analyzed data and contributed to the writing of the final manuscript.

DECLARATION OF INTERESTS

The authors declare no competing interests.

Received: October 16, 2018
Revised: April 22, 2019
Accepted: June 12, 2019
Published: July 18, 2019

REFERENCES

1. Somssich, M., Je, B.I., Simon, R., and Jackson, D. (2016). CLAVATA-WUSCHEL signaling in the shoot meristem. Development *143*, 3238–3248.
2. Caggiano, M.P., Yu, X., Bhatia, N., Larsson, A., Ram, H., Ohno, C.K., Sappl, P., Meyerowitz, E.M., Jönsson, H., and Heisler, M.G. (2017). Cell type boundaries organize plant development. eLife *6*, e27421.
3. Dello Ioio, R., Nakamura, K., Moubayidin, L., Perilli, S., Taniguchi, M., Morita, M.T., Aoyama, T., Costantino, P., and Sabatini, S. (2008). A genetic framework for the control of cell division and differentiation in the root meristem. Science *322*, 1380–1384.
4. Gaillochet, C., Stiehl, T., Wenzl, C., Ripoll, J.J., Bailey-Steinitz, L.J., Li, L., Pfeiffer, A., Miotk, A., Hakenjos, J.P., Forner, J., et al. (2017). Control of plant cell fate transitions by transcriptional and hormonal signals. eLife *6*, e30135.
5. Leibfried, A., To, J.P., Busch, W., Stehling, S., Kehle, A., Demar, M., Kieber, J.J., and Lohmann, J.U. (2005). WUSCHEL controls meristem function by direct regulation of cytokinin-inducible response regulators. Nature *438*, 1172–1175.
6. Matsuzaki, Y., Ogawa-Ohnishi, M., Mori, A., and Matsubayashi, Y. (2010). Secreted peptide signals required for maintenance of root stem cell niche in Arabidopsis. Science *329*, 1065–1067.
7. Shi, B., Guo, X., Wang, Y., Xiong, Y., Wang, J., Hayashi, K.I., Lei, J., Zhang, L., and Jiao, Y. (2018). Feedback from lateral organs controls shoot apical meristem growth by modulating auxin transport. Dev. Cell. *44*, 204–216.
8. Rodriguez-Villalon, A., Gujas, B., Kang, Y.H., Breda, A.S., Cattaneo, P., Depuydt, S., and Hardtke, C.S. (2014). Molecular genetic framework for protophloem formation. Proc. Natl. Acad. Sci. USA *111*, 11551–11556.
9. Truernit, E., Bauby, H., Belcram, K., Barthélémy, J., and Palauqui, J.C. (2012). OCTOPUS, a polarly localised membrane-associated protein, regulates phloem differentiation entry in Arabidopsis thaliana. Development *139*, 1306–1315.
10. Dolan, L., Janmaat, K., Willemsen, V., Linstead, P., Poethig, S., Roberts, K., and Scheres, B. (1993). Cellular organisation of the Arabidopsis thaliana root. Development *119*, 71–84.
11. Scheres, B., Benfey, P., and Dolan, L. (2002). Root development. Arabidopsis Book *1*, e0101.
12. Blilou, I., Xu, J., Wildwater, M., Willemsen, V., Paponov, I., Friml, J., Heidstra, R., Aida, M., Palme, K., and Scheres, B. (2005). The PIN auxin efflux facilitator network controls growth and patterning in Arabidopsis roots. Nature *433*, 39–44.
13. Hobe, M., Müller, R., Grünewald, M., Brand, U., and Simon, R. (2003). Loss of CLE40, a protein functionally equivalent to the stem cell restricting signal CLV3, enhances root waving in Arabidopsis. Dev. Genes Evol. *213*, 371–381.
14. Meng, L., Buchanan, B.B., Feldman, L.J., and Luan, S. (2012). CLE-like (CLEL) peptides control the pattern of root growth and lateral root development in Arabidopsis. Proc. Natl. Acad. Sci. USA *109*, 1760–1765.
15. Stahl, Y., Grabowski, S., Bleckmann, A., Kühnemuth, R., Weidtkamp-Peters, S., Pinto, K.G., Kirschner, G.K., Schmid, J.B., Wink, R.H., Hülsewede, A., et al. (2013). Moderation of Arabidopsis root stemness by CLAVATA1 and ARABIDOPSIS CRINKLY4 receptor kinase complexes. Curr. Biol. *23*, 362–371.
16. Stahl, Y., Wink, R.H., Ingram, G.C., and Simon, R. (2009). A signaling module controlling the stem cell niche in Arabidopsis root meristems. Curr. Biol. *19*, 909–914.
17. Whitford, R., Fernandez, A., Tejos, R., Pérez, A.C., Kleine-Vehn, J., Vanneste, S., Drozdzecki, A., Leitner, J., Abas, L., Aerts, M., et al. (2012). GOLVEN secretory peptides regulate auxin carrier turnover during plant gravitropic responses. Dev. Cell *22*, 678–685.
18. Depuydt, S., Rodriguez-Villalon, A., Santuari, L., Wyser-Rmili, C., Ragni, L., and Hardtke, C.S. (2013). Suppression of Arabidopsis protophloem differentiation and root meristem growth by CLE45 requires the receptor-like kinase BAM3. Proc. Natl. Acad. Sci. USA *110*, 7074–7079.
19. Ito, Y., Nakanomyo, I., Motose, H., Iwamoto, K., Sawa, S., Dohmae, N., and Fukuda, H. (2006). Dodeca-CLE peptides as suppressors of plant stem cell differentiation. Science *313*, 842–845.
20. Kinoshita, A., Nakamura, Y., Sasaki, E., Kyozuka, J., Fukuda, H., and Sawa, S. (2007). Gain-of-function phenotypes of chemically synthetic CLAVATA3/ESR-related (CLE) peptides in Arabidopsis thaliana and Oryza sativa. Plant Cell Physiol. *48*, 1821–1825.
21. Hazak, O., Brandt, B., Cattaneo, P., Santiago, J., Rodriguez-Villalon, A., Hothorn, M., and Hardtke, C.S. (2017). Perception of root-active CLE peptides requires CORYNE function in the phloem vasculature. EMBO Rep. *18*, 1367–1381.
22. Bleckmann, A., Weidtkamp-Peters, S., Seidel, C.A., and Simon, R. (2010). Stem cell signaling in Arabidopsis requires CRN to localize CLV2 to the plasma membrane. Plant Physiol. *152*, 166–176.
23. Somssich, M., Ma, Q., Weidtkamp-Peters, S., Stahl, Y., Felekyan, S., Bleckmann, A., Seidel, C.A., and Simon, R. (2015). Real-time dynamics of peptide ligand-dependent receptor complex formation in planta. Sci. Signal. *8*, ra76.
24. Anne, P., and Hardtke, C.S. (2018). Phloem function and development-biophysics meets genetics. Curr. Opin. Plant Biol. *43*, 22–28.
25. Lavrekha, V.V., Pasternak, T., Ivanov, V.B., Palme, K., and Mironova, V.V. (2017). 3D analysis of mitosis distribution highlights the longitudinal

zonation and diarch symmetry in proliferation activity of the Arabidopsis thaliana root meristem. Plant J. *92*, 834–845.

26. Furuta, K.M., Yadav, S.R., Lehesranta, S., Belevich, I., Miyashima, S., Heo, J.O., Vatén, A., Lindgren, O., De Rybel, B., Van Isterdael, G., et al. (2014). Plant development. Arabidopsis NAC45/86 direct sieve element morphogenesis culminating in enucleation. Science *345*, 933–937.
27. Czyzewicz, N., Wildhagen, M., Cattaneo, P., Stahl, Y., Pinto, K.G., Aalen, R.B., Butenko, M.A., Simon, R., Hardtke, C.S., and De Smet, I. (2015). Antagonistic peptide technology for functional dissection of CLE peptides revisited. J. Exp. Bot. *66*, 5367–5374.
28. Rodriguez-Villalon, A., Gujas, B., van Wijk, R., Munnik, T., and Hardtke, C.S. (2015). Primary root protophloem differentiation requires balanced phosphatidylinositol-4,5-biphosphate levels and systemically affects root branching. Development *142*, 1437–1446.
29. Marhava, P., Bassukas, A.E.L., Zourelidou, M., Kolb, M., Moret, B., Fastner, A., Schulze, W.X., Cattaneo, P., Hammes, U.Z., Schwechheimer, C., and Hardtke, C.S. (2018). A molecular rheostat adjusts auxin flux to promote root protophloem differentiation. Nature *558*, 297–300.
30. Anne, P., Azzopardi, M., Gissot, L., Beaubiat, S., Hématy, K., and Palauqui, J.C. (2015). OCTOPUS negatively regulates BIN2 to control phloem differentiation in Arabidopsis thaliana. Curr. Biol. *25*, 2584–2590.
31. Breda, A.S., Hazak, O., and Hardtke, C.S. (2017). Phosphosite charge rather than shootward localization determines OCTOPUS activity in root protophloem. Proc. Natl. Acad. Sci. USA *114*, E5721–E5730.
32. Kang, Y.H., Breda, A., and Hardtke, C.S. (2017). Brassinosteroid signaling directs formative cell divisions and protophloem differentiation in Arabidopsis root meristems. Development *144*, 272–280.
33. Kang, Y.H., and Hardtke, C.S. (2016). Arabidopsis MAKR5 is a positive effector of BAM3-dependent CLE45 signaling. EMBO Rep. *17*, 1145–1154.
34. Fiers, M., Golemiec, E., Xu, J., van der Geest, L., Heidstra, R., Stiekema, W., and Liu, C.M. (2005). The 14-amino acid CLV3, CLE19, and CLE40 peptides trigger consumption of the root meristem in Arabidopsis through a CLAVATA2-dependent pathway. Plant Cell *17*, 2542–2553.
35. Müller, R., Bleckmann, A., and Simon, R. (2008). The receptor kinase CORYNE of Arabidopsis transmits the stem cell-limiting signal CLAVATA3 independently of CLAVATA1. Plant Cell *20*, 934–946.
36. Ruiz Sola, M.A., Coiro, M., Crivelli, S., Zeeman, S.C., Schmidt Kjølner Hansen, S., and Truernit, E. (2017). OCTOPUS-LIKE 2, a novel player in Arabidopsis root and vascular development, reveals a key role for OCTOPUS family genes in root metaphloem sieve tube differentiation. New Phytol. *216*, 1191–1204.
37. Rodrigues, A., Santiago, J., Rubio, S., Saez, A., Osmont, K.S., Gadea, J., Hardtke, C.S., and Rodriguez, P.L. (2009). The short-rooted phenotype of the brevis radix mutant partly reflects root abscisic acid hypersensitivity. Plant Physiol. *149*, 1917–1928.
38. Kurihara, D., Mizuta, Y., Sato, Y., and Higashiyama, T. (2015). ClearSee: a rapid optical clearing reagent for whole-plant fluorescence imaging. Development *142*, 4168–4179.
39. Wahl, M., Koberling, F., Patting, M., Rahn, H., and Erdmann, R. (2004). Time-resolved confocal fluorescence imaging and spectrocopy system with single molecule sensitivity and sub-micrometer resolution. Curr. Pharm. Biotechnol. *5*, 299–308.
40. Voinnet, O., Rivas, S., Mestre, P., and Baulcombe, D. (2003). An enhanced transient expression system in plants based on suppression of gene silencing by the p19 protein of tomato bushy stunt virus. Plant J. *33*, 949–956.
41. Lampropoulos, A., Sutikovic, Z., Wenzl, C., Maegele, I., Lohmann, J.U., and Forner, J. (2013). GreenGate—a novel, versatile, and efficient cloning system for plant transgenesis. PLoS ONE *8*, e83043.

STAR★METHODS

KEY RESOURCES TABLE

REAGENT or RESOURCE	SOURCE	IDENTIFIER
Bacterial and Virus Strains		
Agrobacterium tumefaciens GV3101 pMP90	widely distributed	N/A
Chemicals, Peptides, and Recombinant Proteins		
CLE45 peptide, custom synthesized	Genscript	N/A
CLE40 peptide, custom synthesized	Genscript	N/A
CLE26 peptide, custom synthesized	Genscript	N/A
CLE25 peptide, custom synthesized	Genscript	N/A
CLE21 peptide, custom synthesized	Genscript	N/A
CLE20 peptide, custom synthesized	Genscript	N/A
CLE18 peptide, custom synthesized	Genscript	N/A
CLE16 peptide, custom synthesized	Genscript	N/A
CLE14 peptide, custom synthesized	Genscript	N/A
CLE13 peptide, custom synthesized	Genscript	N/A
CLE11 peptide, custom synthesized	Genscript	N/A
CLE9/10 peptide, custom synthesized	Genscript	N/A
CLV3 peptide, custom synthesized	Genscript	N/A
Experimental Models: Organisms/Strains		
Arabidopsis thaliana Col-0 wild-type background	widely distributed	N/A
Nicotiana benthamiana	widely distributed	N/A
Saccharomyces cerevisiae NMY51	Dual System Biotech	N/A
Arabidopsis thaliana BAM3::NLS-3XVENUS transgenic line	this study	N/A
Oligonucleotides		
PP2A-A3 qPCR forward GCA ATC TCT CAT TCC GAT AGT C	Microsynth	N/A
PP2A-A3 qPCR reverse ATA CCG AAC ATC AAC ATC TGG	Microsynth	N/A
actin qPCR forward CCC TCG TAG ATT GGC ACA GT	Microsynth	N/A
actin qPCR reverse GCC ATC CAA GCT GTT CTC TC	Microsynth	N/A
BAM3 qPCR forward CGT CGT TTT AGC TGT GGT CA	Microsynth	N/A
BAM3 qPCR reverse TGC AAC TTC TTC TCC GTT TG	Microsynth	N/A
Software and Algorithms		
GraphPad Prism version 7.0e	GraphPad software	N/A

LEAD CONTACT AND MATERIALS AVAILABILITY

Further information and requests for resources and reagents should be directed to and will be fulfilled by the Lead Contact, Christian S. Hardtke (christian.hardtke@unil.ch). There are no restrictions to the availability of reagents.

EXPERIMENTAL MODEL AND SUBJECT DETAILS

Plant materials and growth conditions

Arabidopsis thaliana Columbia-0 (Col-0) was used as the wild-type for phenotypic analyses and is the background of all mutants investigated: *ops-2* [9]; *brx-2* [37]; *bam3-2* [18]; *ops*^{E319K} [8]; the *clv2* allele *rlp10-1* and *crn-10* [21]. Transgenic constructs used in this study have been described before [8, 18, 21, 28, 31], except *BAM3::NLS-3XVENUS*, which was a gift from Dr. P. Cattaneo. Seeds were surface sterilized, germinated and grown vertically under continuous light at 22°C on 0.5X Murashige and Skoog media supplemented with 0.8% or 1% agar, and 0.3% or 1.0% sucrose (media was homogeneous within a given experiment).

METHOD DETAILS

Quantitative real-time PCR

To determine *BAM3* expression levels, 5mm root tips were collected from 7-day-old seedlings for total RNA extraction (QIAGEN), and cDNAs were produced by reverse transcriptase (Invitrogen). Quantitative real-time PCR was performed in triplicate on three biological replicates (Data S1) using MESA Blue qPCR MasterMix Plus for SYBR assay Low Rox (Eurogentec). *PP2A-A3* and *ACTIN* were used as reference genes (primers 5′-GCA ATC TCT CAT TCC GAT AGT C-3′ + 5′-ATA CCG AAC ATC AAC ATC TGG-3′ and 5′-CCC TCG TAG ATT GGC ACA GT-3′ + 5′-GCC ATC CAA GCT GTT CTC TC-3′, respectively). *BAM3* transcripts were quantified using primers 5′-CGT CGT TTT AGC TGT GGT CA-3′ and 5′-TGC AAC TTC TTC TCC GTT TG-3′.

Physiological assays

All assays were performed in tissue culture under the growth conditions specified above. CLE peptides were obtained from a commercial supplier (Genscript), synthesized at > 80% purity, diluted in water and used at final concentration as indicated. For root length measurements, plates were scanned at 600 dpi resolution, and seedling root length was determined using Fiji software. To investigate OPS protein stability, 5-day-old seedlings were transferred to media containing 50 μM of the protein synthesis inhibitor cycloheximide. At the end of the treatment, the seedlings were transferred to fixation solution (4% paraformaldehyde in 1X PBS) for one hour, washed with 1X PBS and cleared with ClearSee solution [38]. One hour before imaging, samples were incubated with Calcofluor white solution (0.2% in ClearSee solution) to stain the cell walls. Fluorescence intensity of OPS-GFP or OPS^{E319K}-GFP was measured at the plasma membrane of protophloem cells using the segmented line tool of the Fiji software. The raw measurements of the assays are available in Data S1.

Reporter detection and microscopy

GUS reporter staining was performed as described previously [18, 28]. Fluorescent protein signals were acquired by confocal microscopy using Zeiss LSM 700, 710 or 880 inverted confocal scanning microscopes following standard procedures [21, 31]. Pictures were taken with 20 × or 40 × water/oil immersion objectives. For comparisons, samples were grown in parallel and analyzed on the same day, with identical microscopy settings, unless indicated otherwise.

FRET/FLIM interaction studies

For the initial FRET-FLIM studies, leaves of 4-week-old *Nicotiana benthamiana* plants were co-infiltrated with *A. tumefaciens* cultures carrying T-DNA constructs of CRN-CFP together with either CLV2-CITRINE, OPS-CITRINE, or CLV2-CITRINE and OPS-CITRINE, all expressed under the *35S* promoter. The fluorescence lifetime of CRN-CFP was measured in these leaves after 2 and 3 days at the plasma membrane of transformed epidermis cells, using a Leica SP8 with the PicoHarp 300 TCSPC Module and a pulsed 440 nm laser at 10 kHz. At last 1000 counts/pixel were acquired for 25 images for every co-infiltration. The recorded decay plots were fitted against a erythrosine B decay plot using an exponential reconvolution model (n = 2) [39] for lifetime calculations.

The subsequent lifetime analyses were performed in a transient *Nicotiana benthamiana* expression system, using plants cultivated 4 weeks under standard greenhouse conditions before infiltration of leaves with *Agrobacterium tumefaciens* strain GV3101 pMP90 harboring the silencing suppressor p19 [40] and the expression plasmids for the fluorophore-tagged proteins of interest. The Gateway compatible vectors pABindGFP and pABindmCh [22] provide an estradiol-inducible transgene activation mechanism and were completed via LR-reaction with the coding regions of *CRN* (At5G13290), *CLV2* (AT1G65380), *BAM3* (At4g20270), *OPS* (AT3G09070), and *FLS2* (AT5G46330) as a plasma membrane-localized negative control. For constitutive expression under the *UBQ10* or the *35S* promoter, additional transgenes were constructed using GreenGate cloning [41]. The BAM3 deletion construct encompassed amino acids 1 to 691. The CRN deletion construct encompassed amino acids 1 to 93. *A. tumefaciens* strains were cultivated overnight and adjusted to an OD_{600nm} of 0.3 each in 5% (w/v) sucrose, 450μM acetosyringone, and 0.01% (v/v) silwet, and incubated for 2h at 4°C prior to infiltration. After 2-3 days plants were induced by spraying 20μM estradiol + 0.1% Tween-20 and analyzed within 6 to 20 h. For CLE45 treatments, transformed plants were infiltrated with mock (5% sucrose, 0.02% Silwet) or CLE45 solution (5% sucrose, 0.02% Silwet, 10μM CLE45), and FRET/FLIM measurements were performed 5-30 min. immediately after. For FRET/FLIM measurements, a Zeiss confocal laser scanning microscope LSM 780 (40x water immersion objective, Zeiss C-PlanApo, NA 1.2) equipped with a single-photon counting device (PicoQuant Hydra Harp 400) was used. The GFP donor was excited at 485 nm by a linearly polarized diode laser (LDH-D-C-485) working at a frequency of 32 MHz. Excitation power was adjusted to 1 μW. Emission was detected in perpendicular and parallel polarization by Tau-SPADs (PicoQuant) with a band-pass filter (520/35 AHF). Image acquisition was done at zoom 8 with a frame size of 256 × 256 and a pixel dwell time of 12.6 μs, taking 60 frames for each measurement. To calculate the average lifetime of each measurement, further analysis was performed using PicoQuant SymphoTime software applying a biexponential fit. The displayed values are intensity-weighted mean lifetimes τ in ns. Data were obtained from at least 3 independent experiments. The raw measurements of the assays are available in Data S1.

Yeast split ubiquitin assays

Split ubiquitin assays were performed using the DUAL Membrane system (Dual System Biotech). The full coding sequence of OPS was inserted into the pPR3-N vector by SfiI restriction. Truncated versions of BAM3 and CRN were cloned into the pPR3-SUC and pBT3-SUC vectors by SfiI restriction, respectively, such that their target peptide sequence was replaced by the yeast target peptide.

The yeast NMY51 strain was then co-transformed with 250ng of prey and 250ng of bait vectors by thermic shock and selected on SD -LW media. Colonies were transferred onto SD – LWH (+/−3AT) to monitor interactions. Plasma membrane-localized Fur4-NubI was used as a positive control, Fur4-NubG as a negative control.

QUANTIFICATION AND STATISTICAL ANALYSIS

Statistical analyses were performed in Graphpad Prism software, version 7.0e. Details for each pertinent figure panel are available in Data S1.

DATA AND CODE AVAILABILITY

The published article includes all datasets generated or analyzed during this study.